

LETTER TO THE EDITOR

Discovery of the cyclic C₅H radical in TMC-1 [★]

C. Cabezas¹, M. Agúndez¹, R. Fuentetaja¹, Y. Endo², N. Marcelino^{3,4}, B. Tercero^{3,4}, J. R. Pardo¹, P. de Vicente⁴ and J. Cernicharo¹

¹ Grupo de Astrofísica Molecular, Instituto de Física Fundamental (IFF-CSIC), C/ Serrano 121, 28006 Madrid, Spain. e-mail: carlos.cabezas@csic.es; jose.cernicharo@csic.es

² Department of Applied Chemistry, Science Building II, National Yang Ming Chiao Tung University, 1001 Ta-Hsueh Rd., Hsinchu 300098, Taiwan

³ Observatorio Astronómico Nacional (IGN), C/ Alfonso XII, 3, 28014, Madrid, Spain.

⁴ Centro de Desarrollos Tecnológicos, Observatorio de Yebes (IGN), 19141 Yebes, Guadalajara, Spain.

Received; accepted

ABSTRACT

Cyclic C₅H (*c*-C₅H), the radical formed by substituting an ethynyl group CCH for the hydrogen atom in the *c*-C₃H radical, has been detected for the first time in the space. The *c*-C₅H species is an isomer of the well-known linear radical *l*-C₅H and is ~6 kcal/mol less stable. A total of 17 rotational transitions were detected for the *c*-C₅H species in TMC-1 within the 31.0–50.3 GHz range using the Yebes 40m radio telescope. We derive a column density of $(9.0 \pm 0.9) \times 10^{10} \text{ cm}^{-2}$ for *c*-C₅H. Additionally, we observed 12 lines for *l*-C₅H and derive a column density for it of $(1.3 \pm 0.3) \times 10^{12} \text{ cm}^{-2}$, which results in an abundance ratio *c*-C₅H/*l*-C₅H of 0.069. This is in sharp contrast with the value found for the analogue system *c*-C₃H/*l*-C₃H, whose ratio is 5.5 in TMC-1. We discuss the formation of *c*-C₅H and conclude that this radical is probably formed in the reaction of atomic carbon with diacetylene.

Key words. Astrochemistry — ISM: molecules — ISM: individual (TMC-1) — line: identification — molecular data

1. Introduction

Carbon can be considered the most versatile element for building molecules in the interstellar medium (ISM). In fact, about 80% of the nearly 260 molecules detected to date in space (CDMS¹, Müller et al. 2005) contain at least one carbon atom, and one-fourth are hydrocarbons. The chemistry of hydrocarbons is dominated to a large extent by highly unsaturated (low H/C ratios) carbon chain molecules such as the C_{*n*}H family. The hydrocarbon radicals C_{*n*}H detected in space range from the methylene radical, CH (Dunham 1937), to C₈H (Cernicharo & Guélin 1996; Bell et al. 1999). The smaller ones, such as C₂H, C₃H, and C₄H, are observed in star-forming regions (Tucker et al. 1974), photon-dominated regions (Teyssier et al. 2004), cold dark clouds (Wootten et al. 1980; Irvine et al. 1981; Thaddeus et al. 1985), translucent molecular clouds (Turner et al. 2000), circumstellar envelopes (Guélin et al. 1978; Pardo & Cernicharo 2007), and the diffuse medium (Bell et al. 1983; Nyman 1984). The larger ones, C₅H, C₆H, C₇H, and C₈H, are mainly observed in cold dense molecular clouds (Cernicharo et al. 1987; Saito et al. 1987; Bell et al. 1999; Araki et al. 2017) and in the expanding envelope of the carbon-rich star IRC+10216 (Cernicharo et al. 1986a,b; Suzuki et al. 1986; Cernicharo & Guélin 1996; Guélin et al. 1996).

The C₃H radical shows a particular behaviour because it exists in two isomeric forms, a cyclic one (*c*-C₃H) and a linear one (*l*-C₃H), with *c*-C₃H lower in energy. Both have been widely ob-

served in the ISM, and in general the *c*-C₃H isomer (Yamamoto et al. 1987; Mangum & Wootten 1990; Turner et al. 2000; Cernicharo et al. 2000; Zhang et al. 2009; Liszt et al. 2014) is found to have a larger abundance than *l*-C₃H (Thaddeus et al. 1985; Turner et al. 2000; Pardo & Cernicharo 2007). The C₅H radical is predicted to adopt up to seven different structures, including linear, cyclic, and bent ones (Crawford et al. 1999). Conversely to C₃H, the linear structure, *l*-C₅H, is the most stable one. It has been detected in the ISM by Cernicharo et al. (1986a,b, 1987). The cyclic isomer, *c*-C₅H, which is analogous to the *c*-C₃H isomer but with the H atom replaced by a ethynyl (-CCH) group, is the second most stable isomer (6.1 kcal/mol; Crawford et al. 1999). As *l*-C₅H (McCarthy et al. 1999), *c*-C₅H was characterized in the laboratory (Apponi et al. 2001), but it had not yet been detected in the ISM.

In this Letter we report the detection of the *c*-C₅H radical towards the cold dark cloud TMC-1. The derived abundance is compared with that of the linear isomer *l*-C₅H, and the plausible reactions that could lead to the formation of this species are discussed with the aid of a chemical model.

2. Observations

The observational data used in this article consist of spectra of TMC-1 taken with the Yebes 40m telescope towards the cyanopolyne peak of TMC-1, $\alpha_{J2000} = 4^{\text{h}}41^{\text{m}}41.9^{\text{s}}$ and $\delta_{J2000} = +25^{\circ}41'27.0''$. The observations are part of the ongoing QUI-JOTE² line survey (Cernicharo et al. 2021a) carried out during different observing runs between November 2019 and January

[★] Based on observations carried out with the Yebes 40m telescope (projects 19A003, 20A014, 20D023, and 21A011). The 40m radio telescope at Yebes Observatory is operated by the Spanish Geographic Institute (IGN; Ministerio de Transportes, Movilidad y Agenda Urbana).

¹ <https://cdms.astro.uni-koeln.de/>

² Q-band Ultrasensitive Inspection Journey to the Obscure TMC-1 Environment.

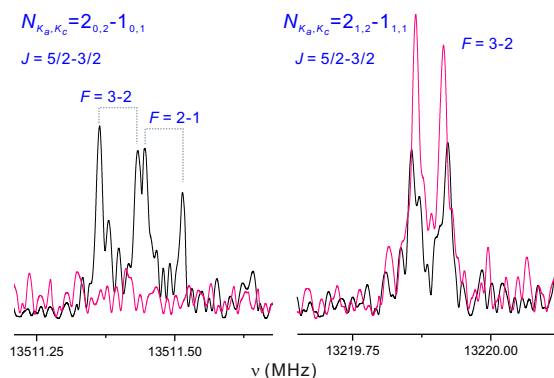


Fig. 1. FTMW spectra for $c\text{-C}_5\text{H}$. Coloured lines show spectra using argon (magenta) and neon (black) as the carrier gas in the supersonic expansion. Each line is split into two Doppler components because the direction of the supersonic jet expansion is parallel to the standing wave in the Fabry-Pérot cavity of the spectrometer. The difference in the magnitude of Doppler splitting when different carrier gases – neon and argon – are used is related to the velocity of the molecule in the jet; it is reciprocal to the square root of the atomic mass of the carrier gas.

2022. The observations were performed using the frequency-switching mode with a frequency throw of 10 MHz in the very first observing runs, in November 2019 and February 2020, 8 MHz in the observations of January–November 2021, and 10 MHz again in the last observing run that took place between October 2021 and January 2022. The total on-source telescope time is 430 h in each polarization (twice this value after averaging the two polarizations), which can be split into 238 and 192 hours for the 8 MHz and 10 MHz frequency throws. The QUIJOTE line survey uses a 7 mm receiver covering the Q band (31.0–50.3 GHz) with horizontal and vertical polarizations. Receiver temperatures in 2019 and 2020 varied from 22 K at 32 GHz to 42 K at 50 GHz. In 2021, some power adaptation carried out in the down-conversion chains changed the receiver temperatures to 16 K at 32 GHz and 25 K at 50 GHz. The backends are 16 Fourier transform spectrometers, which provide a bandwidth of 8×2.5 GHz in each polarization, thus covering practically the whole Q band, with a spectral resolution of 38.15 kHz. The system is described in detail by Tercero et al. (2021).

The intensity scale used is antenna temperature, T_A^* , which is calibrated using two absorbers at different temperatures and the ATM package (Cernicharo 1985; Pardo et al. 2001). Calibration uncertainties were assumed to be 10% based on the observed repeatability of the line intensities between different observing runs. All data were analysed using the software GILDAS³.

3. Results

3.1. New laboratory data for $c\text{-C}_5\text{H}$

Apponi et al. (2001) observed the rotational spectrum of the $c\text{-C}_5\text{H}$ radical in the laboratory. It has a 2B_2 electronic ground state with C_{2v} symmetry. Owing to the Bose statistics of the two equivalent off-axis carbon nuclei, only rotational levels with odd K_a occur, and rotational transitions with $K_a=0$ are thus forbidden. Apponi et al. (2001) found two series of lines, with $K_a=0$ and $K_a=1$ values, which were fitted separately. The $K_a=1$ series was ascribed to the ground state of $c\text{-C}_5\text{H}$, while the origin of the $K_a=0$ lines was not totally clear. Our hypothesis is that the $K_a=0$ lines arise from a low frequency vibrationally excited

state with different vibrational symmetry (either B_1 or B_2) from that for the ground state (A_1). To gain some insight into this, we carried out Fourier transform microwave (FTMW) spectroscopy experiments using as carrier gases either neon or argon.

The rotational spectrum of the $c\text{-C}_5\text{H}$ radical was observed using a Balle-Flygare narrow-band-type FTMW spectrometer operating in the frequency region 4–40 GHz (Endo et al. 1994; Cabezas et al. 2016). We observed some of the rotational transitions reported before by Apponi et al. (2001). The short-lived species $c\text{-C}_5\text{H}$ was produced in a supersonic expansion by a pulsed electric discharge of a gas mixture of C_2H_2 (0.3%) diluted in neon or argon. The gas mixture was flowed through a pulsed-solenoid valve that is accommodated in the backside of one of the cavity mirrors and aligned parallel to the optical axis of the resonator. A pulse voltage of 1000 V with a duration of 450 μs was applied between stainless-steel electrodes attached to the exit of the pulsed discharge nozzle, resulting in an electric discharge synchronized with the gas expansion. The resulting products generated in the discharge were then probed by FTMW spectroscopy, which allowed small hyperfine splittings to be resolved.

Previous studies have shown that heavier inert gases have an enhanced cooling efficiency in supersonic expansions due to the larger collision energies they provide (Cabezas et al. 2018). Consequently, an argon-seeded expansion is expected to favour the population of the lower frequency vibrational states, while higher vibrational states will be populated in a neon-seeded expansion. Figure 1 shows the spectra recorded using argon and neon gases. When argon is used, only the $K_a=1$ lines are observed, but in the neon experiments both $K_a=0$ and $K_a=1$ are observed. We note that the intensity of the $K_a=1$ lines decreases when neon is used due to a fraction of its population being distributed between higher vibrationally excited states. In light of our experimental observations, we infer that the $K_a=0$ series of lines come from a low frequency vibrationally excited state, probably an in-plane or out-of-plane bending mode (Crawford et al. 1999).

3.2. Identification of $c\text{-C}_5\text{H}$ in TMC-1

Line identification in this work was done using the catalogues MADEX (Cernicharo 2012), CDMS (Müller et al. 2005), and JPL (Pickett et al. 1998). As of May 2022, the MADEX code contained 6434 spectral entries corresponding to the ground and vibrationally excited states, together with the corresponding isotopologues, of 1734 molecules. Once the assignment of all known molecules and their isotopologues is done, QUIJOTE will permit us to search for molecules for which frequencies are known. Moreover, QUIJOTE also allows us to perform rotational spectroscopy in space of new species for which no previous rotational spectroscopic laboratory information is available, such as HC_5NH^+ (Marcelino et al. 2020), HC_3O^+ (Cernicharo et al. 2020a), HC_3S^+ (Cernicharo et al. 2021b), CH_3CO^+ (Cernicharo et al. 2021c), HCCS^+ (Cabezas et al. 2022a), C_5H^+ (Cernicharo et al. 2022), HC_7NH^+ (Cabezas et al. 2022b), and HCCNCH^+ (Agúndez et al. 2022).

Only the $K_a=1$ series of lines of $c\text{-C}_5\text{H}$ are expected to be observed in TMC-1. We used the rotational parameters reported by Apponi et al. (2001) to predict, using the SPFIT program (Pickett 1991), the frequency transition lines in the Q band. We used a dipole moment of 3.39 D, following Crawford et al. (1999). The molecule was implemented in the MADEX code (Cernicharo 2012), which was used to search for the $K_a=1$ lines. A total of 17 lines of $c\text{-C}_5\text{H}$ were detected in TMC-1 above the 3σ level;

³ <http://www.iram.fr/IRAMFR/GILDAS/>

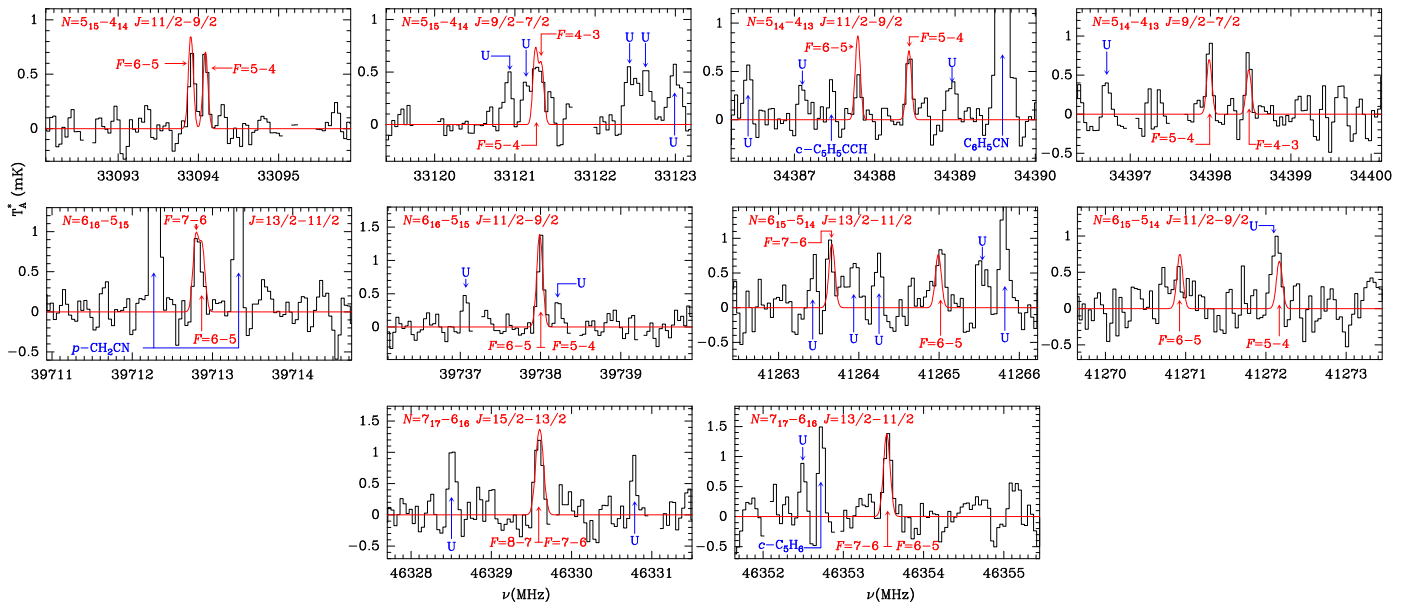


Fig. 2. Observed lines of c -C₅H in TMC-1 in the 31.0-50.3 GHz range. Frequencies and line parameters are given in Table 1. Quantum numbers for the observed transitions are indicated in each panel. The red line shows the synthetic spectrum computed for a rotational temperature of 6 K and a column density of $9.0 \times 10^{10} \text{ cm}^{-2}$ (see text). Blanked channels correspond to negative features created in the folding of the frequency-switching data. The label U corresponds to unidentified features above 4σ .

Table 1. Observed line parameters for c -C₅H in TMC-1.

$N'_{K'_a, K'_c} \leftarrow N_{K_a, K_c}$	Transition $J' \leftarrow J$	$F' \leftarrow F$	ν_{obs}^a (MHz)	$\int T_A^* dv^b$ (mK km s ⁻¹)	Δv^c (km s ⁻¹)	T_A^* (mK)
$5_{1,5} \leftarrow 4_{1,4}$	$11/2 \leftarrow 9/2$	$6 \leftarrow 5$	33093.924	0.58 ± 0.09	0.79 ± 0.14	0.69 ± 0.11
$5_{1,5} \leftarrow 4_{1,4}$	$11/2 \leftarrow 9/2$	$5 \leftarrow 4$	33094.088	0.50 ± 0.08	0.62 ± 0.14	0.75 ± 0.11
$5_{1,5} \leftarrow 4_{1,4}$	$9/2 \leftarrow 7/2$	$5 \leftarrow 4$	33121.256	0.50 ± 0.06	0.86 ± 0.09	0.55 ± 0.11
$5_{1,5} \leftarrow 4_{1,4}$	$9/2 \leftarrow 7/2$	$4 \leftarrow 3$	33121.338	0.28 ± 0.05	0.64 ± 0.08	0.41 ± 0.11
$5_{1,4} \leftarrow 4_{1,3}$	$11/2 \leftarrow 9/2$	$6 \leftarrow 5$	34387.798	0.33 ± 0.07	0.66 ± 0.17	0.46 ± 0.10
$5_{1,4} \leftarrow 4_{1,3}$	$11/2 \leftarrow 9/2$	$5 \leftarrow 4$	34388.431	0.54 ± 0.08	0.72 ± 0.12	0.70 ± 0.10
$5_{1,4} \leftarrow 4_{1,3}$	$9/2 \leftarrow 7/2$	$5 \leftarrow 4$	34397.987	0.72 ± 0.12	0.68 ± 0.14	1.00 ± 0.20
$5_{1,4} \leftarrow 4_{1,3}$	$9/2 \leftarrow 7/2$	$4 \leftarrow 3$	34398.472	0.55 ± 0.11	0.60 ± 0.14	0.86 ± 0.20
$6_{1,6} \leftarrow 5_{1,5}$	$13/2 \leftarrow 11/2$	$7 \leftarrow 6$	39712.806	0.67 ± 0.12	0.60 ± 0.14	1.05 ± 0.19
$6_{1,6} \leftarrow 5_{1,5}$	$13/2 \leftarrow 11/2$	$6 \leftarrow 5$	39712.830	0.67 ± 0.18	0.76 ± 0.18	0.83 ± 0.19
$6_{1,6} \leftarrow 5_{1,5}$	$11/2 \leftarrow 9/2$	$6 \leftarrow 5$	39738.002	0.91 ± 0.09	0.64 ± 0.08	1.34 ± 0.14
$6_{1,6} \leftarrow 5_{1,5}$	$11/2 \leftarrow 9/2$	$5 \leftarrow 4$				
$6_{1,5} \leftarrow 5_{1,4}$	$13/2 \leftarrow 11/2$	$7 \leftarrow 6$	41263.639	0.65 ± 0.22	0.60 ± 0.22	1.02 ± 0.23
$6_{1,5} \leftarrow 5_{1,4}$	$13/2 \leftarrow 11/2$	$6 \leftarrow 5$	41265.018	0.83 ± 0.27	0.90 ± 0.38	0.87 ± 0.23
$6_{1,5} \leftarrow 5_{1,4}$	$11/2 \leftarrow 9/2$	$6 \leftarrow 5$	41270.899	0.44 ± 0.12	0.77 ± 0.27	0.54 ± 0.23
$6_{1,5} \leftarrow 5_{1,4}$	$11/2 \leftarrow 9/2$	$5 \leftarrow 4$	41272.163	0.45 ± 0.08^d	0.55 ± 0.28	0.76 ± 0.23
$7_{1,7} \leftarrow 6_{1,6}$	$15/2 \leftarrow 13/2$	$8 \leftarrow 7$	46329.587	0.85 ± 0.17	0.66 ± 0.13	1.22 ± 0.25
$7_{1,7} \leftarrow 6_{1,6}$	$15/2 \leftarrow 13/2$	$7 \leftarrow 6$				
$7_{1,7} \leftarrow 6_{1,6}$	$13/2 \leftarrow 11/2$	$7 \leftarrow 6$				
$7_{1,7} \leftarrow 6_{1,6}$	$13/2 \leftarrow 11/2$	$6 \leftarrow 5$	46353.556	1.01 ± 0.22	0.69 ± 0.17	1.37 ± 0.25

Notes. ^(a) Observed frequencies towards TMC-1 for which we adopted a v_{LSR} of 5.83 km s^{-1} . The frequency uncertainty is 10 kHz. ^(b) Integrated line intensity in mK km s^{-1} . ^(c) Full width at half maximum derived by fitting a Gaussian function to the observed line profile (in km s^{-1}). ^(d) Line overlaps with an unidentified line.

they are shown in Fig. 2. These 17 lines correspond to 20 hyperfine components, three of which are not resolved, from five $K_a=1$ rotational transitions with $N=5, 6,$ and 7 . The derived line parameters are given in Table 1. A fit to the observed line profiles assuming a source diameter of $40''$ (Fossé et al. 2001) provides a rotational temperature of $6.0 \pm 0.5 \text{ K}$ and a column density of $N(c\text{-C}_5\text{H}) = (9.0 \pm 0.9) \times 10^{10} \text{ cm}^{-2}$. The synthetic spectra are compared with observations in Fig. 2 (red line). No lines with $K_a=0$ were detected, which is in line with our conclusion that those lines belong to a vibrationally excited state that would be under-populated in TMC-1 due to the low kinetic temperature of the cloud.

Using the new observed frequencies in TMC-1 and those measured in the laboratory (Apponi et al. 2001), we have derived, using the SPFIT program (Pickett 1991), a new set of molecular constants for $c\text{-C}_5\text{H}$, which are shown in Table 2. The new molecular constants are practically identical to those provided by Apponi et al. (2001), with the exception of the dipole-dipole constants, $T_{aa}^{(H)}$ and $T_{bb}^{(H)}$. We believe that the definition of these parameters in the fitting code used by Apponi et al. (2001) may be different to that employed by the Pickett program, used in this work, which results in the values being different.

We also observed several lines for the $l\text{-C}_5\text{H}$ isomer. A total of 12 hyperfine components for the $J=15/2-13/2, 17/2-15/2,$ and

Table 2. Spectroscopic parameters of c -C₅H (all in MHz).

Parameter	Lab + TMC-1 ^a	Laboratory ^b
A	45018.0 ^c	45018(20)
B	3504.062107(299) ^d	3504.0621(3)
C	3246.94141(37)	3246.9414(4)
$\Delta_N \times 10^3$	0.2888(52)	0.288 ^e
ε_{aa}	165.1446(216)	165.15(2)
ε_{bb}	5.1476(56)	5.152(6)
ε_{cc}	-28.1469(38)	-28.148(4)
$a_F^{(H)}$	-11.8018(140)	-11.79(2)
$T_{aa}^{(H)}$	6.1686(234)	12.13(7)
$T_{bb}^{(H)}$	-0.170(49)	5.8(1)
σ (kHz)	9.4	-
N_{lines}	42	34

Notes. (a) Merged molecular parameters from a fit to the laboratory and TMC-1 frequencies. (b) Molecular parameters derived by Apponi et al. (2001). (c) Fixed to the previous determined value. (d) Fixed to the previous determined value. (e) Numbers in parentheses are 1σ uncertainties in units of the last digits. (e) Fixed to the C₅H₂ ring chain value; see Apponi et al. (2001).

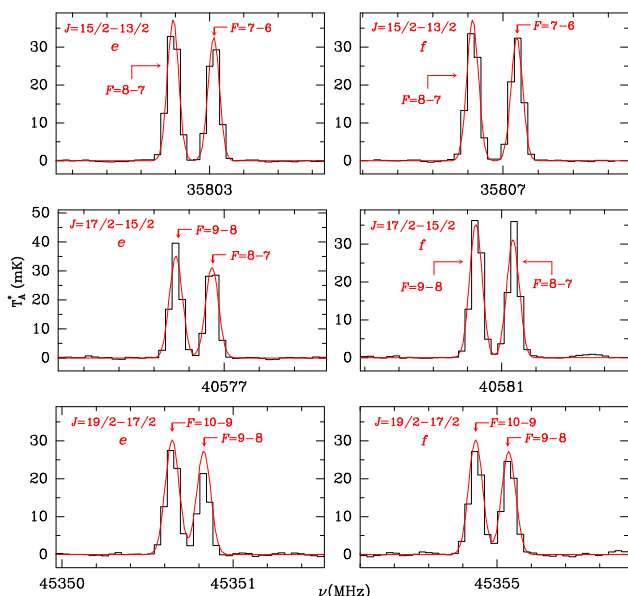


Fig. 3. Observed lines of C₅H in TMC-1 in the 31.0-50.3 GHz range. Frequencies and line parameters are given in Table 3. Quantum numbers for the observed transitions are indicated in each panel. The red line shows the synthetic spectrum computed for a rotational temperature of 6 K and a column density of 1.3×10^{12} cm⁻² (see text). Blanked channels correspond to negative features created in the folding of the frequency-switching data.

19/2-17/2 transitions, which belong to the $^2\Pi_{1/2}$ spin sub-level, were detected (see Fig. 3 and Table 3) with antenna temperatures around 30 mK. An analysis of the line intensities through a line model fitting procedure (Cernicharo et al. 2021d) provides a rotational temperature of 6.0 ± 0.5 K and a column density of $N(l\text{-C}_5\text{H}) = (1.3 \pm 0.3) \times 10^{12}$ cm⁻². We assumed a dipole moment of 4.88 D for $l\text{-C}_5\text{H}$ (Woon 1995). Therefore, the abundance ratio $c\text{-C}_5\text{H}/l\text{-C}_5\text{H}$ is 0.069 in TMC-1. This value is far from that found in TMC-1 for the analogue system $c\text{-C}_3\text{H}/l\text{-C}_3\text{H}$, whose ratio is 5.5 (Loison et al. 2017).

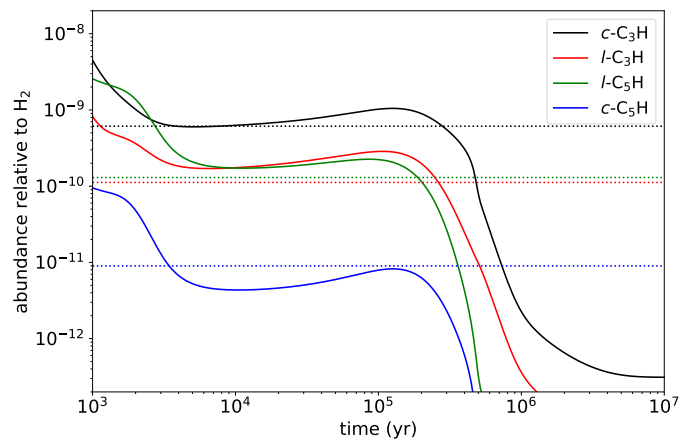
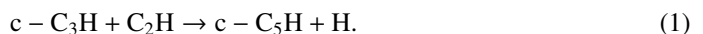


Fig. 4. Calculated fractional abundances of the cyclic and linear isomers of C₃H and C₅H as a function of time. The abundances observed in TMC-1 for the isomers of C₃H (Loison et al. 2017) and C₅H (this study) are indicated by dotted horizontal lines.

4. Chemistry

In order to shed some light on the formation of $c\text{-C}_5\text{H}$ in TMC-1, we carried out gas-phase chemical modelling calculations similar to those presented in Cabezas et al. (2021). Briefly, we adopted physical conditions typical of cold dark clouds: a volume density of H nuclei of 2×10^4 cm⁻³, a gas kinetic temperature of 10 K, a visual extinction of 30 mag, a cosmic-ray ionization rate of H₂ of 1.3×10^{-17} s⁻¹, and the so-called set of low-metal elemental abundances (e.g., Agúndez & Wakelam 2013). We employed the chemical network RATE12 from the UMIST database (McElroy et al. 2013), which has been updated with results from Lin et al. (2013) and expanded with the subset of gas-phase chemical reactions involving C₃H and C₃H₂ isomers revised by Loison et al. (2017).

The cyclic isomer of C₅H is not included in either the UMIST (McElroy et al. 2013) or KIDA (Wakelam et al. 2015) databases, and information on reactions involving it are lacking in the literature. Our main aim here is thus to explore whether plausible reactions of formation of $c\text{-C}_5\text{H}$ can account for the abundance observed in TMC-1. Since $c\text{-C}_5\text{H}$ can be viewed as the result of substituting an H atom in $c\text{-C}_3\text{H}$ with a C₂H group, an obvious reaction of formation of $c\text{-C}_5\text{H}$ is



We thus included this reaction with a rate coefficient of 3×10^{-10} cm³ s⁻¹, which is similar to rate coefficients measured at low temperature for other reactions of C₂H with closed-shell unsaturated hydrocarbons (Chastaing et al. 1998). Another interesting potential source of $c\text{-C}_5\text{H}$ is the reaction between atomic carbon and diacetylene,



where both the linear and cyclic isomers of C₅H are in principle possible, although chemical networks only consider the linear isomer as product (Smith et al. 2004; Loison et al. 2014). Reaction (2) is thought to occur rapidly at low temperatures based on experimental studies of reactions of C with closed-shell unsaturated hydrocarbons such as C₂H₂ (Chastaing et al. 2001). Takahashi (2000) studied this reaction theoretically and concluded that both the linear and cyclic isomers of C₅H can be formed

Table 3. Observed line parameters for *l*-C₅H in TMC-1.

Transition		Parity	ν_{obs}^a (MHz)	$\int T_A^* dv^b$ (mK km s ⁻¹)	$\Delta\nu^c$ (km s ⁻¹)	T_A^* (mK)
$J' \leftarrow J$	$F' \leftarrow F$					
15/2←13/2	8←7	<i>e</i>	35802.786	26.79±0.13	0.70± 0.01	36.19±0.17
15/2←13/2	7←6	<i>e</i>	35803.024	23.10±0.13	0.68± 0.01	31.81±0.17
15/2←13/2	8←7	<i>f</i>	35806.828	26.36±0.09	0.69± 0.01	35.73±0.14
15/2←13/2	7←6	<i>f</i>	35807.078	24.00±0.09	0.69± 0.01	32.69±0.14
17/2←15/2	9←8	<i>e</i>	40576.724	22.85±0.19	0.54± 0.01	39.42±0.20
17/2←15/2	8←7	<i>e</i>	40576.931	20.37±0.20	0.57± 0.01	33.53±0.20
17/2←15/2	9←8	<i>f</i>	40580.854	23.55±0.17	0.58± 0.01	38.45±0.15
17/2←15/2	8←7	<i>f</i>	40581.071	20.82±0.17	0.55± 0.01	35.62±0.15
19/2←17/2	10←9	<i>e</i>	45350.645	18.04±0.15	0.58± 0.01	29.00±0.20
19/2←17/2	9←8	<i>e</i>	45350.829	12.68±0.15	0.55± 0.01	21.63±0.20
19/2←17/2	10←9	<i>f</i>	45354.877	17.68±0.20	0.60± 0.01	27.80±0.35
19/2←17/2	9←8	<i>f</i>	45355.070	16.07±0.20	0.59± 0.01	25.66±0.35

Notes. ^(a) Observed frequencies towards TMC-1 for which we adopted a v_{LSR} of 5.83 km s⁻¹. The frequency uncertainty is 10 kHz. ^(b) Integrated line intensity in mK km s⁻¹. ^(c) Full width at half maximum derived by fitting a Gaussian function to the observed line profile (in km s⁻¹).

without an entrance barrier. On the other hand, calculations by Sun et al. (2008) show that only the linear isomer of C₅H should be formed. The different conclusions are likely due to the fact that reaction (2b) was found to be exothermic by 1 kcal mol⁻¹ by Takahashi (2000) but endothermic by 0.7 kcal mol⁻¹ by Sun et al. (2008). That is, formation of *c*-C₅H is nearly thermo-neutral. Here we assume that reaction (2b) occurs with a branching ratio of just 10%. Finally, we assumed that *c*-C₅H reacts fast with neutral atoms (H, C, N, and O) and cations that are known or expected to be abundant in TMC-1, such as C⁺ and HCO⁺.

In Fig. 4 we show the calculated abundances of the cyclic and linear isomers of C₃H and C₅H. It is seen that the peak calculated abundances, reached in the 10⁵-10⁶ yr time range, agree well with the observed values. If we focus on cyclic C₅H, according to the chemical model the main reaction of formation is C + C₄H₂. That is, if this reaction produces cyclic C₅H with only a branching ratio of 10%, then it can by itself explain the abundance of *c*-C₅H observed in TMC-1. Further studies to evaluate the branching ratios of the reaction C + C₄H₂ would allow the chemistry of the linear and cyclic isomers of C₅H in cold dark clouds to be better constrained.

5. Conclusions

We have reported the first identification of the *c*-C₅H radical towards TMC-1. We observed 17 rotational transitions within the 31.0–50.3 GHz range using the Yebes 40m radio telescope. The derived *c*-C₅H/*l*-C₅H abundance ratio of 0.069 is very different from that found for *c*-C₃H/*l*-C₃H, whose ratio is 5.5 in TMC-1. A state-of-the-art chemical model reproduces the observed abundance of *c*-C₅H and indicates that this radical can probably be formed in the reaction of atomic carbon with diacetylene.

Acknowledgements. We acknowledge funding support from Spanish Ministerio de Ciencia e Innovación through grants PID2019-106110GB-I00, PID2019-107115GB-C21, and PID2019-106235GB-I00 and from the European Research Council (ERC Grant 610256: NANOCOSMOS). We would like to thank María Eugenia Sanz for her useful comments on the laboratory experiments of *c*-C₅H radical.

References

Agúndez, M., & Wakelam, V. 2013, *Chem. Rev.*, 113, 8710
 Agúndez, M., Cabezas, C., Marcelino, N. et al. 2022, *A&A*, 659, L9
 Apponi, A. J., Sanz, M. E., Gottlieb, C. A., et al. 2001, *ApJL*, 547, L65
 Araki, M., Takano, S., Sakai, N., et al. 2017, *ApJ*, 847, 51
 Bell, M. B., Feldman, P. A., & Matthews, H. E. 1983, *ApJ*, 273, L35

Bell, M. B., Feldman, P. A., Watson, J. K. G., et al. 1999, *ApJ*, 518, 740
 Cabezas, C., Guillemin, J.-C., & Endo, Y. 2016, *J. Chem. Phys.*, 145, 184304
 Cabezas, C., Guillemin, J.-C., & Endo, Y. 2018, *J. Chem. Phys.*, 149, 084309
 Cabezas, C., Tercero, B., Agúndez, M., et al. 2021, *A&A*, 650, L9
 Cabezas, C., Agúndez, M., Marcelino, N. et al. 2022a, *A&A*, 657, L4
 Cabezas, C., Agúndez, M., Marcelino, N. et al. 2022b, *A&A*, 659, L8
 Cernicharo, J. 1985, Internal IRAM report (Granada: IRAM)
 Cernicharo, J., Kahane, K., Gómez-González, J., & Guélin, M. 1986a, *A&A*, 164, L1
 Cernicharo, J., Kahane, K., Gómez-González, J., & Guélin, M. 1986b, *A&A*, 167, L5
 Cernicharo, J., Guélin, M., & Walmsley, C. M. 1987, *A&A*, 172, L5
 Cernicharo, J., & Guélin, M. 1996, *A&A*, 309, L27
 Cernicharo, J., Guélin, M., & Kahane, C. 2000, *A&ASuppl. Ser.*, 142, 181
 Cernicharo, J. 2012, in *European Conference on Laboratory Astrophysics*, eds. C. Stehlé, C. Joblin, & L. d'Hendecourt, EAS Publication Series, 58, 251
 Cernicharo, J., Marcelino, N., Agúndez, M., et al. 2020a, *A&A*, 642, L17
 Cernicharo, J., Agúndez, M., Kaiser, R., et al. 2021a, *A&A*, 652, L9
 Cernicharo, J., Cabezas, C., Endo, Y., et al. 2021b, *A&A*, 646, L3
 Cernicharo, J., Cabezas, C., Bailleux, S., et al. 2021c, *A&A*, 646, L7
 Cernicharo, J., Agúndez, M., Cabezas, C., et al. 2021d, *A&A*, 649, L15
 Cernicharo, J., Agúndez, M., Cabezas, C. et al. 2022, *A&A*, 657, L16
 Chastaing, D., James, P. L., Sims, I. R., & Smith, I. W. M. 1998, *Faraday Discuss.*, 109, 165
 Chastaing, D., Le Picard, S., Sims, I. R., & Smith, I. W. M. 2001, *A&A*, 365, 241
 Crawford, T. D., Stanton, J. F., Saeh, J. C., & Schaefer, H. F. 1999, *JACS*, 121, 1902
 Dunham, Jr., T. 1937, *PASP*, 49, 26
 Endo, Y., Kohguchi, H., & Ohshima, Y. 1994, *Faraday Discuss.*, 97, 341.
 Fossé, D., Cernicharo, J., Gerin, M., & Cox, P. 2001, *ApJ*, 552, 168
 Guélin, M., Green, S., & Thaddeus, P. 1987, *ApJ*, 224, L27
 Guélin, M., Cernicharo, J., Travers, M. J., et al. 1996, *A&A*, 317, L1
 Irvine, W. M., Hoglund, B., Friberg, P., et al. 1981, *ApJL* 248, L113
 Lin, Z., Talbi, D., Roueff, E., et al. 2013, *ApJ*, 765, 80
 Liszt, H. S., Pety, J., Gerin, M., & Lucas, R. 2014, *A&A*, 564, A64
 Loison, J.-C., Wakelam, V., Hickson, K. M., et al. 2014, *MNRAS*, 437, 930
 Loison, J.-C., Agúndez, M., Wakelam, V., et al. 2017, *MNRAS* 470, 4075
 Nyman, L.-Å. 1984, *ApJ*, 141, 323
 Marcelino, N., Agúndez, M., Tercero, B. et al. 2020, *A&A*, 643, L6
 Mangum, J. G., & Wootten, A. 1990, *A&A*, 239, 319
 McCarthy, M. C., Chen, W., Apponi, A. J., et al. 1999, *ApJ*, 520, 158
 McElroy, D., Walsh, C., Markwick, A. J., et al. 2013, *A&A*, 550, A36
 Müller, H.S.P., Schlöder, F., Stutzki, J., & Winnewisser, G. 2005, *J. Mol. Struct.*, 742, 215
 Pardo, J. R., & Cernicharo, J. 2007, *ApJ*, 654, 978
 Pardo, J. R., Cernicharo, J., & Serabyn, E. 2001, *IEEE Trans. Antennas and Propagation*, 49, 12
 Pickett, H. M. 1991, *J. Mol. Spectr.*, 148, 371
 Pickett, H.M., Poynter, R. L., Cohen, E. A., et al. 1998, *J. Quant. Spectrosc. Radiat. Transfer*, 60, 883
 Saito, S., Kawaguchi, K., Suzuki, H. et al. 1987, *PASJ*, 39, 193
 Smith, I. W. M., Herbst, E., & Chang, Q. 2004, *MNRAS*, 350, 323
 Sun, B. J., Huang, C. Y., Kuo, H. H., et al. 2008, *J. Chem. Phys.*, 128, 244303
 Suzuki, H., Ohishi, M., Kaifu, N. et al. 1986, *PASJ*, 38, 911
 Takahashi, J. 2000, *PASJ*, 52, 401
 Tercero, F., López-Pérez, J. A., Gallego, J. D., et al. 2021, *A&A*, 645, A37
 Teyssier, D., Fossé, D., Gerin, M., et al. 2004, *A&A*, 417, 135
 Thaddeus, P., Gottlieb, C. A., Hjalmarson, A., et al. 1985, *ApJ*, 294, L49
 Tucker, K. D., Kutner, M. L., & Thaddeus, P. 1974, *ApJ*, 193, L115
 Turner, B. E., Herbst, E., & Terzieva, R. 2000, *ApJS*, 126, 427
 Wakelam, V., Loison, J.-C., Herbst, E., et al. 2015, *ApJS*, 217, 20
 Woon, D. E. 1995, *Chem. Phys. Lett.*, 244, 45
 Wootten, A., Bozyan, E. P., Garrett, D. B., et al. 1980, *ApJ*, 239, 944
 Yamamoto, S., Saito, S., Ohishi, M., et al. 1987, *ApJ*, 322, L55
 Zhang, Y., Kwok, S., & Nakashima, J.-I. 2009, *ApJ*, 700, 1262